

# Probabilistic Contact Estimation and Impact Detection for State Estimation of Quadruped Robots

Marco Camurri\*, Maurice Fallon†, Stéphane Bazeille‡, Andreea Radulescu\*,  
Victor Barasuol\*, Darwin G. Caldwell\*, and Claudio Semini\*

\* Department of Advanced Robotics, Istituto Italiano di Tecnologia, Genoa, Italy. `firstname.lastname@iit.it`

† School of Informatics, University of Edinburgh, Edinburgh, UK. `maurice.fallon@ed.ac.uk`

‡ IRCCyN, Ecole des Mines de Nantes, Nantes, France. `stephane.bazeille@emn.fr`

**Abstract**—Reliable state estimation is crucial for the stable planning and control of legged locomotion. A fundamental component of a state estimator in legged platforms is given by Leg Odometry, which only requires information about kinematics and contacts. To detect ground contact many legged robots use dedicated sensors on each foot. However, this choice is impractical for many agile legged robots in field operations, as these sensors often degrade and break. Instead, this paper focuses on the development of a robust Leg Odometry module, which does not require contact sensing. The module can infer foot impacts using internal force sensing and use this knowledge to improve the kinematics-inertial state estimate of the robot’s body. We show how our approach can reach comparable performance to systems with foot sensors. Extensive experimental results lasting over one hour are presented with our 85 kg quadrupedal robot HyQ, carrying out a variety of gaits.

## I. INTRODUCTION

Legged robots present unique capabilities for traversing a multitude of rough terrains, where they can potentially outperform wheeled or tracked systems. The successful implementation of these capabilities depends on the robot’s ability to generate viable body trajectories, using a self-estimated base state vector, computed in real-time on board the robot.

Reliable control and locomotion of a legged robotic system requires an estimate of position, orientation, linear and angular velocities, and acceleration of its base. This state vector is used for navigation, balancing, push recovery, local mapping and the planning of body trajectories.

The essential sensor inputs for self-reliant base pose estimation in legged robots typically include an inertial measurement unit (IMU) — measuring accelerations and angular velocity — and joint encoders, which are used to compute position and velocity of the end effectors (*i.e.*, the robot’s feet) through forward kinematics.

Reliable velocity estimates for the base can be extracted from the feet velocities expressed in the base frame, a technique known as Leg Odometry (LO) [1]. Typical approaches use constraints based on the knowledge of at least one secure (*i.e.*, non-slipping) contact between the feet and the ground. Detecting such a contact event is not trivial, as it depends on the amount of frictional force the foot exerts on the terrain [2]. According to the Coulomb model of dry friction, this is directly proportional to the normal component of the Ground

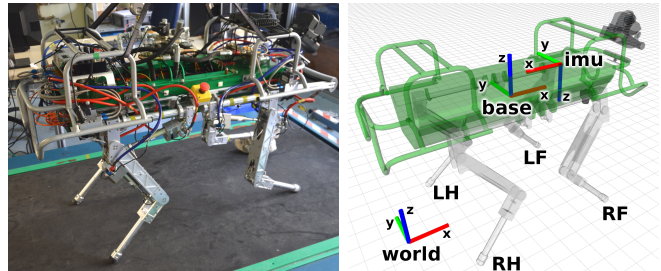


Fig. 1: *Left*: IIT’s Hydraulic Quadruped robot (HyQ). *Right*: Summary of the coordinate frames and abbreviations used in this paper: the Base frame is attached to the geometric center of the robot’s torso and has  $x$ -axis (red) pointing forward,  $y$ -axis (green) pointing on the left, and  $z$ -axis (blue) pointing up; the IMU frame is also attached to the base link, with a different orientation; the World frame is a fixed reference frame. The legs are referred by the following abbreviations: LF (Left Front), RF (Right Front), LH (Left Hind), RH (Right Hind).

Reaction Force (GRF) and the foot-terrain static friction coefficient, which is generally unknown. Additionally, impact forces play a critical role, as they can cause slippage [3] and exacerbate undesired compliances in the leg structure. Furthermore, when contact sensors at the feet are unavailable, the difficulty of the task increases, as an indirect estimate of the GRF is required.

This paper addresses these issues by providing a novel method for reliable detection and estimation of contacts between the feet and the ground. Estimated contacts are used to fuse the individual leg contributions to the estimated base velocity using a probabilistic approach. Our technique is based on estimation of the GRF at foot level, which provides a degree of confidence that a foot is firmly in contact with the ground. With this information, our method resulted in state-of-the-art performance on a dynamic quadruped robot, executing quasi-static and dynamic locomotion gaits.

We present the performance of the method on the Hydraulic Quadruped (HyQ) [4], a dynamic platform capable of a variety of locomotion gaits including trotting up to 2 m/s and multi-directional crawling. Figure 1 depicts the HyQ platform and a schematic showing the coordinate frames used in this paper

and feet naming conventions. We present results for the proposed kinematic state and stance estimator in a variety of dynamic and quasi-static locomotion experiments with a total duration of 62 min. To our best knowledge, this constitutes the most extensive study and assessment of kinematics-inertial state estimation on heavy and dynamic legged systems, to date.

The remainder of this paper is structured as follows: Section II lists the relevant literature on the topic; Section III provides a formal definition of the proposed state estimation problem which does not require contact sensing; Section IV describes our approach to contact estimation. In Section V we describe how linear velocity measurement updates are created using this contact information; Section VI describes our experimental setup as well as extensive test results; in Section VII we discuss about the effect of leg compliance on the experimental results and the algorithmic limitations of our approach, before concluding in Section VIII with a summary and some suggestions for future work.

## II. RELATED WORK

State estimation of legged robots is a widely studied problem. A variety of solutions have been proposed with different sensor combinations including [5]–[7]. We are however most interested in larger scale platforms, that can perform dynamic gaits, such as trotting or running, without contact sensors, and can carry a substantial payload. In this context, to the best of our knowledge, the available literature either addresses legged state estimation with contact sensors or contact/collision estimation without contact sensors.

### A. Legged State Estimation with Contact Sensors

Recently, Blösch *et al.* [8] developed a state estimator that fuses leg kinematics and inertial information using an Extended Kalman Filter (EKF). The state vector includes the feet positions, whose uncertainty is used to account for moderate slippage and absence of ground contacts, which are detected with dedicated sensors. The validity of this approach was demonstrated on the medium-sized quadruped robot StarLETH [9] for a 1 min straight crawl. Later, the authors [10] extended their work by replacing the EKF with an Unscented Kalman Filter (UKF) and redefining the formulation of the state vector to be robot-centric (*i.e.*, referred to the base frame, which is attached to the robot, instead of the world frame, attached to the fixed earth). The velocity contributions of each leg readings are discarded if the filter innovation, expressed in Mahalanobis distance, exceeds a fixed threshold, which was found empirically. This procedure eliminates the impact of spurious filter updates originating from legs whose contact state estimates are unreliable. As in [8], the performance of the approach was demonstrated on the StarLETH platform, for a 23 s trot on a flat terrain made unstable and slippery by placing wooden debris along the way.

In [11], Fallon *et al.* presented Pronto: an efficient, modular and open-source EKF-based state estimator. The algorithm uses an IMU-based process model and combines this with measurement corrections from different sensor modalities

(LO, LiDAR and vision) to produce a position estimate for the humanoid robot Atlas, developed by Boston Dynamics. In particular, the LO module handles contacts using a Schmitt trigger (a two threshold comparator with hysteresis, see [12]) on the contact sensor signals: the contact is detected when the low threshold is crossed and it is released when an arbitrary time has passed and the high threshold is crossed. When the robot is in double support, only one leg is used, for simplicity. The filter is able to handle out-of-order and asynchronous inputs from different sensors. Originally developed for the DARPA Robotics Challenge, its implementation has been recently publicly released<sup>1</sup>. We use this filtering framework as a basis of the sensor fusion presented herein. We have replaced the humanoid specific LO module with a quadrupedal specific approach which uses the generated kinematics library of [13] and fuses multiple leg contributions to create raw base velocity estimates.

Ma *et al.* [14] fuse the information from a stereo camera with leg kinematics and a tactical grade IMU through an EKF. The state vector is defined as an error matrix (values propagated from IMU against measurement updates). The approach is focused on visual inertial fusion with LO measurements expressed as delta positions between two key frames, used only in case of failure of the Visual Odometry (VO). The approach produced a robust performance with an error below 1% of the distance traveled when fused with GPS.

### B. Contact/Collision Estimation without Contact Sensors

Most research in the area of contact estimation are focused on collision avoidance for safe Human Robot Interaction (HRI) with manipulators. De Luca *et al.* [15] proposed a collision detection and reaction method which identifies external forces acting on a link as first order filtered external torques acting on the manipulator’s joints. The reaction strategy typically involves stopping or moving the link away and along the direction of the identified contact. Haddadin *et al.* [16] extended this work by introducing a modified version of the contact detection, more recovery strategies, and by extensively experimenting with a human subject.

More recently, Hwangbo *et al.* [17] developed a probabilistic approach for contact estimation for control on the quadruped electric robot ANYmal. The method fuses information about dynamics, differential kinematics and kinematics using a method similar to a Hidden Markov Model (HMM) to reconstruct the contact status. The validity of this approach was demonstrated by comparing their method with Generalized Momentum (GM) approaches, using the detection delay from OptoForce sensors response as a metric.

It has to be noted that the contact detection methods presented above aim to detect the contact as early as possible, in order to promptly take counter measures against unwanted collision [15], [16] or to control the robot [17]. In contrast, we are interested in detecting the first instant of a leg’s contact phase from which a reliable and trustworthy velocity measure

<sup>1</sup><https://github.com/ipab-slmc/pronto-distro>

can be produced, which is a substantially different goal. This is achieved by: 1) learning the threshold of the normal component of the GRF that minimizes the velocity error with the ground truth; 2) incorporating impact information and mutual leg agreement in the covariance associated with the measurement update of the filter.

### III. PROBLEM DEFINITION

The robot base state vector is defined by:

$$\mathcal{X} = [{}^w\mathbf{x}_b \quad {}^b\dot{\mathbf{x}}_b \quad {}^b\ddot{\mathbf{x}}_b \quad {}^w\boldsymbol{\theta}_b \quad {}^b\boldsymbol{\omega}_b \quad \mathbf{b}_a \quad \mathbf{b}_\omega] \quad (1)$$

where the base velocity  ${}^b\dot{\mathbf{x}}_b$ , acceleration  ${}^b\ddot{\mathbf{x}}_b$  and rotational rate  ${}^b\boldsymbol{\omega}_b$  are expressed in the base frame  $b$ , while the position  ${}^w\mathbf{x}_b$  and orientation  ${}^w\boldsymbol{\theta}_b$  are expressed in the fixed world frame  $w$ . The list of frames and their location on HyQ is depicted in Fig. 1. The state vector is completed by IMU acceleration/angular velocity biases  $\mathbf{b}_a$ ,  $\mathbf{b}_\omega$ , and is updated by an EKF, from [11].

Measurements of acceleration and angular velocity are taken from the IMU at 500 Hz. These are transformed into the base frame to produce direct measurements of the base acceleration  ${}^b\ddot{\mathbf{x}}_b$  and angular velocity  ${}^b\boldsymbol{\omega}_b$  as follows:

$${}^b\boldsymbol{\omega}_b = R_i^b {}^i\boldsymbol{\omega}_b = R_i^b {}^i\boldsymbol{\omega}_i \quad (2)$$

$${}^b\ddot{\mathbf{x}}_b = R_i^b {}^i\ddot{\mathbf{x}}_i - b\mathbf{g} \quad (3)$$

where  $R_i^b$  is the rotation matrix from IMU frame  $i$  to the base frame  $b$ . In (3), we assume the effects of angular acceleration and centripetal force (see [18]) to be negligible. The EKF is then propagated using a direct inertial process model.

During the filter update step, a measure for the base velocity  ${}^b\dot{\mathbf{x}}_b$  is computed by fusing a kinematic contribution  ${}^b\dot{\mathbf{x}}_{b_l}$  from each foot  $f_l$ , as follows:

$${}^b\dot{\mathbf{x}}_{b_l} = -{}^b\dot{\mathbf{x}}_{f_l} - {}^b\boldsymbol{\omega}_b \times {}^b\mathbf{x}_{f_l}, \quad (4)$$

where  ${}^b\boldsymbol{\omega}_b$  is computed from (2) and  ${}^b\dot{\mathbf{x}}_{f_l}$ ,  ${}^b\mathbf{x}_{f_l}$  are velocity and position of foot  $f_l$  in the base frame, respectively.

To solve the problem of computing a filter update of  ${}^b\dot{\mathbf{x}}_b$  from each contribution  ${}^b\dot{\mathbf{x}}_{b_l}$ , we need to know which feet are in stable contact with the ground and to then fuse the individual leg contributions into a single EKF measurement update, with associated covariance.

### IV. CONTACT ESTIMATION

We define the contact status for a foot belonging to leg  $l \in \{\text{LF, RF, LH, RH}\}$  as  $S_l \in \{0, 1\}$ , where 1 indicates a reliable stance (*i.e.*, with no motion relative to the ground) and 0 indicates swing or slipping contact. Let  $\mathbf{f}_l$  be the GRF for leg  $l$ . This is either measured with some degree of uncertainty or, in our case, computed from the joint position  $\mathbf{q}_l$ , velocity  $\dot{\mathbf{q}}_l$  and effort  $\boldsymbol{\tau}_l$ , as follows:

$$\mathbf{f}_l = -(J_l^T(\mathbf{q}_l))^{-1}(\boldsymbol{\tau}_l - \mathbf{h}_l(\mathbf{q}_l, \dot{\mathbf{q}}_l, b\mathbf{g})) \quad (5)$$

where  $J_l^T(\mathbf{q}_l)$  is the Jacobian transpose that maps from joint to Cartesian space and  $\mathbf{h}_l(\mathbf{q}_l, \dot{\mathbf{q}}_l, b\mathbf{g})$  is the vector of Centrifugal/Coriolis/gravity torques for leg  $l$ , computed using Recursive Newton-Euler algorithms, as described in [19].

Given the small mass of HyQ's legs compared to the torso, we assume the effect of inertial torques as negligible, compared to the numerical error of computing  $\ddot{\mathbf{q}}$ .

Given  $\mathbf{f}_l = (f_{l,x}, f_{l,y}, f_{l,z})$  and following the definition of [20], the quantity:

$$\mu_f = \frac{\sqrt{f_{l,x}^2 + f_{l,y}^2}}{f_{l,z}}, \quad \forall f_{l,z} > 0 \quad (6)$$

defines a metric to evaluate the robustness, in terms of contact stability, of a foothold. This metric is equal to the actual static friction coefficient  $\mu_s$  when the lateral components of the GRF, denoted with  $f_{l,x}$ ,  $f_{l,y}$ , have a value beyond which the foot would start slipping. Although  $\mu_s$  is unknown, any value of  $\mu_f < \mu_s$  would yield a stable contact, and in particular, the smaller  $\mu_f$  is, the more likely the foot is firmly on the ground. Hence, the quality of contact for a foot related to leg  $l$  at time  $k$  is non-linearly proportional to  $\mathbf{f}_l^k$ . For simplicity and numerical stability, instead of accounting for all the terms of  $\mu_s$ , we ignore the lateral components of  $\mathbf{f}_l^k$ , and assume that, above a certain threshold of  $f_{l,z}^k$ , the frictional force will be sufficient to produce a stable, reliable contact.

To learn this threshold, we model the probability of a reliable ground contact  $P_k$  using a discriminative logit model:

$$P_k(S_l = 1 | \mathbf{f}_l^k) = \frac{1}{1 + \exp(-\beta f_{z,l}^k - \beta_0)} \quad (7)$$

where  $f_{z,l}^k$  is the normal component of the GRF at time  $k$  for leg  $l$ , while  $\beta$  and  $\beta_0$  can be regarded as the weights of a logistic regression classifier. The weights are computed by maximum likelihood estimation on a training set of data collected from characteristic motions, as described next.

#### A. Fitting with Simulated Data

We performed preliminary tests of our approach on data generated by simulation, with contact ground truth. The presented methodology was applied for two distinctive locomotion styles: a static crawl and a dynamic trot.

The crawl gait was obtained using a deliberate planning controller, as depicted in the experiments in [21]. The trot gait was generated using the reactive controller framework presented in [22]. In our experiments the movement was generated using a step frequency of 1.7 Hz, a duty factor of 0.5 and a leg stiffness of  $8.55 \times 10^3$  N/m.

Figure 2 and 3 depict — for crawl and trot logs — the GRF signal (top plot), the fitting of the model against the ground truth for the test set (middle plot), and the obtained logistic function (bottom plot). As expected, the threshold for contact activation in the trot gait is higher (by approx. 20 N). This is due to the fact that for this locomotion gait two legs are off the ground at a time, compared to just one in the crawl.

#### B. Fitting with Real Data

To test the classifier in a real scenario, we performed training on half of a trot log and half of a crawl log from our dataset (see Section VI-B) and we used the rest of the dataset as a test set for the learned model.

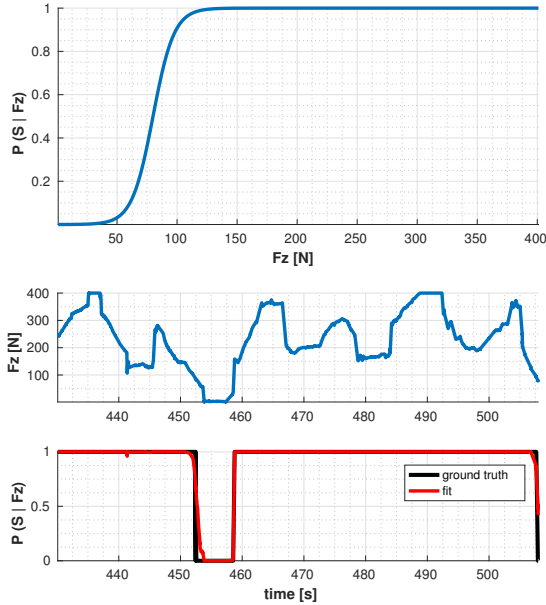


Fig. 2: Crawl gait simulation. *Top plot*: learned logistic model function. *Middle plot*: normal component of the GRF for one leg. *Bottom plot*: learned stance probability and ground truth

As no suitable commercial solution for contact sensing was available on our hardware, the ground truth for the training was defined as the time sequence of stance leg combinations that minimized the error between estimated and true base velocities. Additional post-processing was applied to maintain the continuity of swing and stance intervals. This approach also has the advantage that the classifier tends to learn the force threshold beyond which the associated velocity measurement produced by the foot in question becomes reliable.

Fig. 4 and 5 display, for crawl and trot respectively, the obtained logistic function (top plot), the GRF signal (middle plot), and the fitting of the model against the ground truth for the test set (bottom plot). As in the simulation, the threshold for contact activation in the trot gait is higher, with a larger difference compared to the simulated gaits.

We compared state estimation performance using our contact estimation approach against two other thresholding methods on  $f_{z,l}$ : a single threshold method and a Schmitt trigger. Table I provides an example of how our approach improves the state estimation performance as a function of per distance traveled in the  $x$ -axis, thanks to the better selection of the stance legs used for the velocity computation. For these experiments, we decoupled the effect of gyro bias and linear position estimate by using the orientation estimate from our Vicon motion capture system. In particular the proposed logistic regression significantly increases the performance of the LO during the trot gait. No improvement is achieved for the crawling gait, as impact events occur less frequently and with reduced intensity.

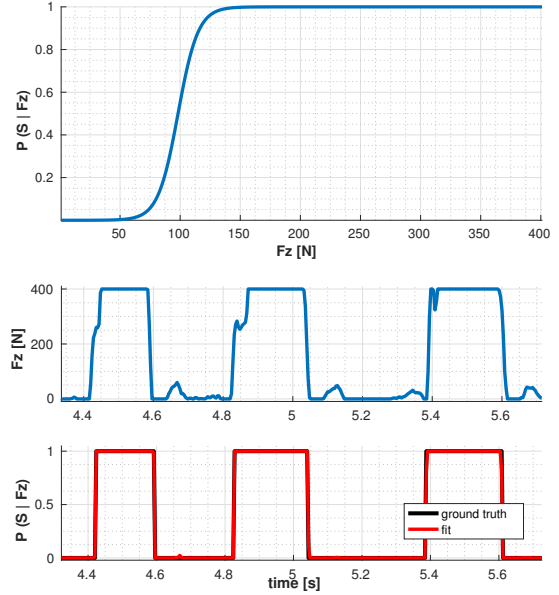


Fig. 3: Trot gait simulation. *Top plot*: learned logistic model function. *Middle plot*: normal component of the GRF for one leg. *Bottom plot*: learned stance probability and ground truth

	Fixed threshold [cm/m]	Hysteresis [cm/m]	Logistic regr. [cm/m]
Crawl	1.34	1.34	1.34
Trot	1.79	0.75	0.43

TABLE I: Comparison between different contact estimators: fixed threshold, Schmitt trigger (hysteresis) and our method (logistic regression). Performance is computed as drift per distance traveled in the  $x$ -axis.

## V. VELOCITY ESTIMATION

Given an estimate of which feet are likely to be in reliable contact, we compute a velocity estimate of the base  ${}_b\dot{\mathbf{x}}_b$  and its associated covariance matrix  $\Sigma_v = \text{diag}(\sigma_x^2, \sigma_y^2, \sigma_z^2)$  using kinematic sensing. This will then be used as a measurement in the EKF update step. To compute the estimate we use the contact estimate introduced in Section IV, while to compute the covariance we leverage the knowledge about the consistency between the velocity contributions of the stance legs and the detection of impacts.

### A. Velocity Computation

To produce a base velocity update for the filter we combine the individual base velocity estimates produced by each leg. We use the probability of a given foot related to leg  $l$  being in contact at time  $k$  as a weighting criteria as follows:

$${}_b\dot{\mathbf{x}}_b(k) = \frac{\sum_{l \in C} P_k(S_l = 1 | \mathbf{f}_l^k) {}_b\dot{\mathbf{x}}_{b_l}(k)}{\sum_{l \in C} P_k(S_l = 1 | \mathbf{f}_l^k)} \quad (8)$$

and  $C$  is the set of feet that exceed the 0.5 threshold of the logistic regressor. Among the feet that are detected to be in contact, weight is given to be proportional to the probability of contact.

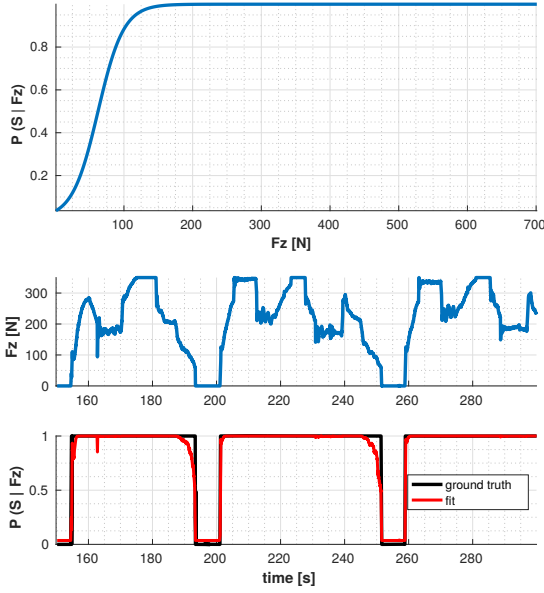


Fig. 4: Crawl gait experiment. *Top plot*: learned logistic model function. *Middle plot*: normal component of the GRF for one leg. *Bottom plot*: learned stance probability and ground truth.

### B. Covariance Estimation

Correctly estimating the covariance of these velocity contributions is particularly important. The robot executes different types of dynamic gaits and creates entirely unrealistic velocity updates when a foot strikes the ground.

To compute the covariance matrix  $\Sigma_v$  associated with each velocity update, we considered two factors: consistency between each contribution  ${}_b\dot{\mathbf{x}}_{b_l}$  and impact forces. For each coordinate  $r \in \{x, y, z\}$  we compute the corresponding variance at a given instant as:

$$\sigma_r^2(k) = \sigma_0^2 + (\alpha_1 \text{std} [{}_b\dot{\mathbf{x}}_{b_l \in C}(k)]_c + (1 - \alpha_1) \alpha_2 |\Delta \bar{f}_z^k|)^2 \quad (9)$$

where:

$$|\Delta \bar{f}_z^k| = \frac{1}{\dim(C)} \sum_{l \in C} |f_{z,l}^k - f_{z,l}^{k-1}| \quad (10)$$

is the average of the absolute difference between the current and previous normal component of the GRF. We use this value as an indicator of an impact event.  $\sigma_0$  is the baseline standard deviation for velocity,  $\text{std} [{}_b\dot{\mathbf{x}}_{b_l \in C}]$  is the  $r$ -th component of the standard deviation of the velocity contributions among stance legs,  $\alpha_1$  is a factor that balances the effects of leg consistency and impacts (we use 0.5) and  $\alpha_2$  is a normalization factor, computed as the ratio between typical velocity error and  $|\Delta \bar{f}_z^k|$  at the same instant.

The middle term of (9) incorporates the fact that legs deemed to be in contact should provide consistent estimates for the same base velocity. The last term takes into consideration the effect of impact forces, which propagate throughout the system and affect also legs that are already in contact (see Fig. 6).

In Fig. 7 we show an example of the adaptive covariance described in this section, on data from a trot log. We compare

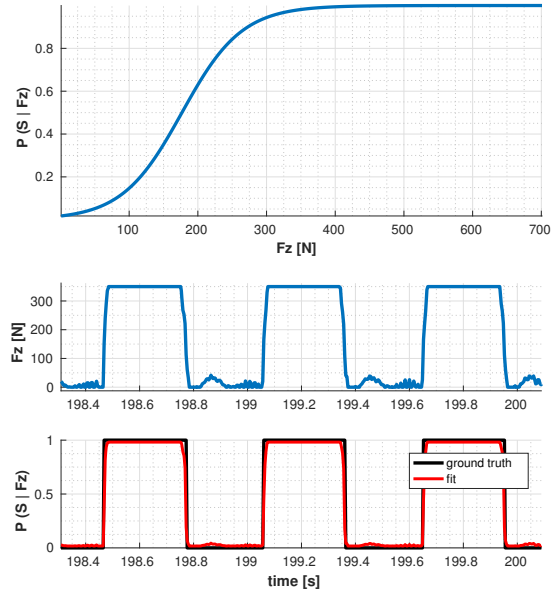


Fig. 5: Trot gait experiment. *Top plot*: learned logistic model function. *Middle plot*: normal component of the GRF for one leg. *Bottom plot*: learned stance probability and ground truth.

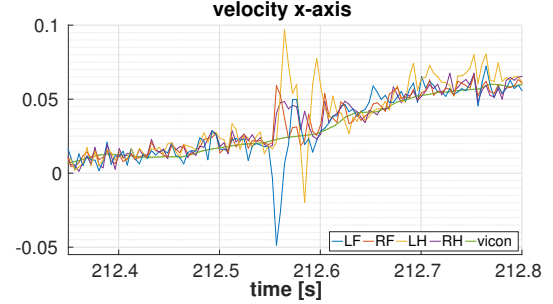


Fig. 6: Effect of impulsive force on estimated velocities during a crawl gait. The Left Hind (LH) leg strikes the ground at time 212.55 s producing unrealistic velocity estimates for that leg — as well as for the other legs, due to propagation of the impact on the rest of the structure.

the raw (*i.e.*, not yet processed by the EKF) base velocity computed from (8) and the ground truth, on the  $x$ -axis. The velocity is colored proportionally to the standard deviation  $\sigma_x(k)$  extracted from (9). Note the change of color in the proximity of feet contact transitions and impacts, where the standard deviation is increased from 0.02 m/s up to 0.15 m/s. During these intervals, the confidence in the velocity updates processed by the EKF is reduced.

## VI. EXPERIMENTS

### A. Experimental Platform

The experimental results were obtained on the torque controlled Hydraulic Quadruped robot (HyQ) [4] which is capable of multiple locomotion gaits. The system is 1 m long, weighs approximately 85 kg and contains 12 actuated revolute joints with a rotational range of  $120^\circ$  each, with a

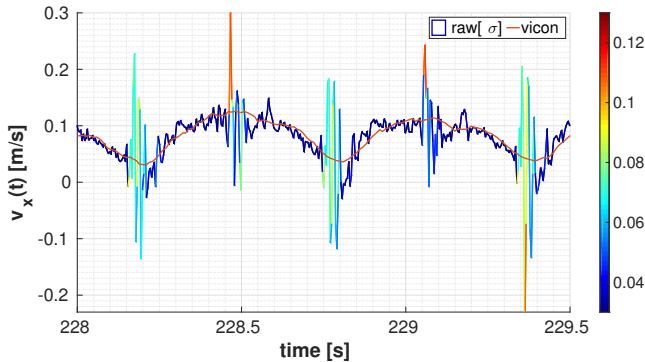


Fig. 7: Raw velocity on  $x$ -axis compared to ground truth during a trot motion. The standard deviation associated to the velocity samples is shown with a color scale, ranging from dark blue (0.03 m/s to dark red 0.13 m/s).

peak torque of 145 N m at a hydraulic pressure of 16 MPa. A brief summary of the sensors on the robot, including accuracy and sampling frequency, is provided in Table II. All the sensor inputs except the ones from the IMU are generated at 1 kHz within a real-time environment, sampled at 250 Hz and transmitted as LCM messages to the filter. The IMU is directly accessed in user-space via USB at 500 Hz and synchronized passively [23].

Sensor Type	Model	Accuracy	Rate
IMU	Microstrain GX3-25	0.5–2.0°	500 Hz
Rel. Encoders	Avago AEDA3300 BE1	0.0045°	250 Hz
Abs. Encoders	ASM AS5045	0.0879°	250 Hz
Force	Burster 8417	±25 N	250 Hz

TABLE II: Sensor specifications

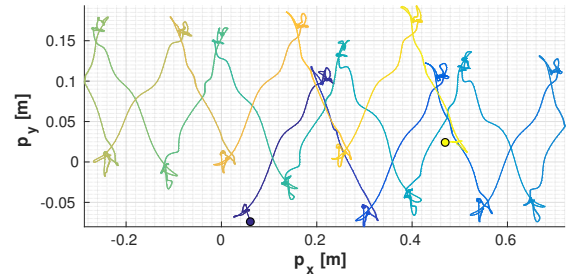
### B. Dataset

The dataset we recorded for the experimental tests is summarized in Table III. It consists of seven runs, three of a trotting gait and four of a crawling gait, for a total duration of 62 min. The total distance traveled was computed by path integral of the robot trajectory from Vicon position measurements at 100 Hz, while the velocity signals are computed by numerical differentiation and de-noised through a delay-compensated second order Savitzky-Golay filter [24], which was preferred over a moving average filter, for its capability of retaining signals which can vary abruptly while removing the noise.

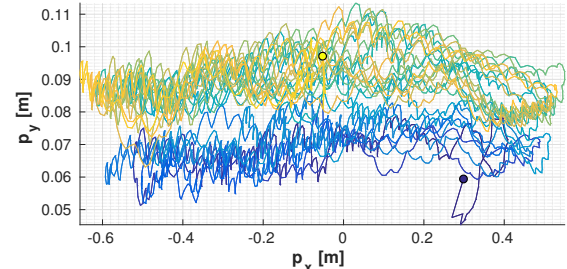
Due to the limited size of our motion capture space, these gaits were performed by repeating forward-backward motions within a  $2.5 \times 1.2 \text{ m}^2$  area. Figures 8a and 8b depict a typical trajectory (projected onto the  $xy$ -plane) of a crawl and a trot run, respectively.

### C. Performance evaluation

Fig. 9 compares, for a forward trot, the velocity estimates before filtering (top plot), after filtering (middle plot) and the ground truth (bottom plot). Despite several spikes due to impacts, the filtered output is smooth, thanks to the adaptive covariance algorithm presented in Section V, which



(a) Crawl trajectory



(b) Trot trajectory

Fig. 8: Typical crawl and trot base trajectories, projected on the  $xy$ -plane. Color changes from dark blue to light yellow indicate the evolution of time. Starting and ending positions are indicated by a blue and a yellow dot, respectively.

Name	Gait	Duration	Distance
trot_1	trot	606 s	38.55 m
trot_2	trot	608 s	40.85 m
trot_3	trot	609 s	48.96 m
walk_1	crawl	395 s	8.05 m
walk_2	crawl	345 s	6.94 m
walk_3	crawl	600 s	10.31 m
walk_4	crawl	600 s	10.89 m

TABLE III: Summary of the dataset.

automatically reduces the confidence on the kinematics filter updates during stance transitions.

In Figs. 10 and 11 we show the average performance on the dataset presented in Section VI-B, with distinction between trot and crawl logs, and between coordinates. In Fig. 10 we evaluate the Drift per Distance Traveled (DDT), *i.e.*, the mean position drift divided by the total distance covered by the robot, while Fig. 11 shows the Root Mean Square error (RMS) of the velocity estimates. We compared the proposed algorithm (yellow bars) with a simple method based on a fixed threshold of 50 N on the normal component of the GRF for contact detection, and static covariance for the velocity updates (dark blue bars).

Although the two gaits we used for our tests differ considerably, for both we noticed a performance degradation on the  $y$ -axis, an issue we attribute to structural flexibility of the leg (see Section VII for more details).

1) *Trot logs:* For the trotting logs (left-hand sides of Figs. 10 and 11), we demonstrate that properly handling impacts improves significantly the performance both in position and velocity. We have achieved this in the  $x$  and the  $z$  axes,

where the error in position is more than halved with respect to the simple method (dark blue bars). In the  $y$  axis the same performance improvement was not achieved due to limb flexibility, as explained in Section VII.

2) *Crawling*: The plots on the right-hand side of Figs. 10 and 11 show the two main performance indicators for the crawling logs. As expected, given the sporadic occurrence of impacts, the improvement provided by our proposed approach is limited. We can notice how the error on the  $z$  component is lower than for the trot because of the continuous support typical for this gait.

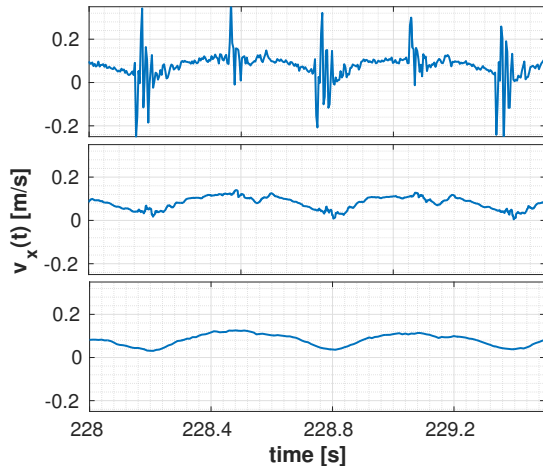


Fig. 9: Example of velocity estimation for a trot log on  $x$ -axis. *Top plot*: raw velocity. *Middle plot*: output of the EKF. *Bottom plot*: ground truth.

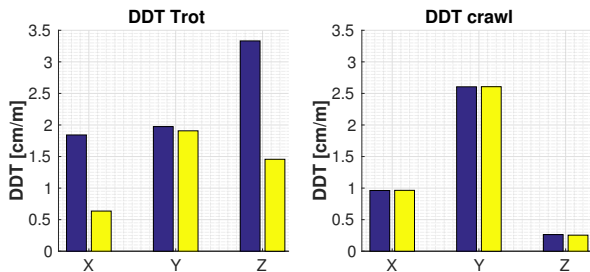


Fig. 10: Drift per Distance Traveled (DDT) for trot and crawl logs. Left blue bars show the baseline method, right yellow bars show our approach.

## VII. DISCUSSION

### A. Leg Flexibility Under Load

Large robots like HyQ can suffer from leg compliance and flexibility when their feet strike the ground, even at slow speeds. Typical forces at the feet are in the range of 200–600 N while crawling or trotting, and beyond 1200 N while bounding. These forces are partially absorbed by the leg structure.

A dedicated experiment allowed us to identify that the major cause of performance degradation along the  $y$ -axis

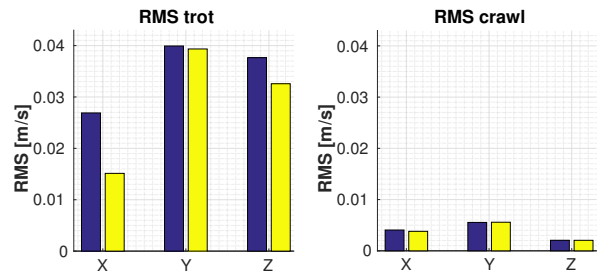


Fig. 11: Velocity Root Mean Square (RMS) error for trot and crawl logs. Left blue bars show the baseline method, right yellow bars show our approach.

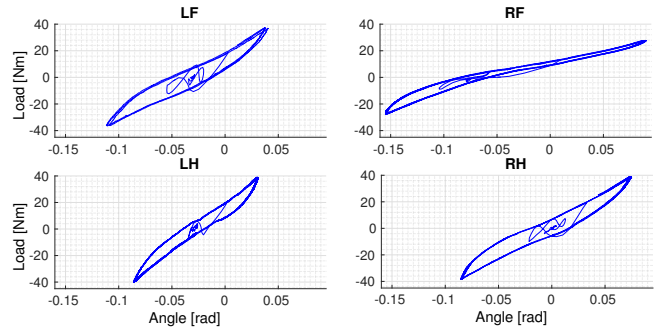


Fig. 12: Joint Load vs. Position plots for the four legs under loading/unloading produced at each foot on the  $y$ -axis. Hysteresis indicates non-linear elasticity and energy dissipation between loading and unloading phases.

(shown in Figs. 10 and 11) is the intrinsic flexibility of the legs on the coronal plane. With the robot base fixed in place and the feet firmly in contact with the ground, we controlled the legs to produce lateral forces at the feet along the  $y$ -axis, using a triangular wave with period of 20 s and intensity of 70 N. Figure 12 shows the relationship between position and applied torque at Hip Abduction Adduction (HAA) joints (*i.e.*, joints rotating around an axis passing through the hip and aligned with the  $x$ -axis), and highlights the nonlinearity of the leg structure and the hysteresis between loading and unloading phases. Given the configuration of the experiment, the joint motion should have been very small, while instead a range up to 0.24 rad is recorded (see widths of the graphs in Fig. 12). This indicates significant structural flexibility.

Methods to model this nonlinearity so as to achieve the same state estimation performance for the  $y$ -axis as was achieved for the  $x$  and  $z$  axes is ongoing research, as well as testing the approach on the second version of HyQ, called HyQ2Max [25], which is expected to show a better structural behavior.

### B. Limitations

Besides the mechanical structure of the robot, limitations lie in a) the training of the contact classifier and b) terrain properties. A specific training procedure was required for each gait, and would be needed for every new gait or loading condition for the legs. This could be avoided by

performing unsupervised learning and active exploration of terrain frictional properties, but at the current stage only tests in controlled single leg setups have been reported in literature [20]. An alternative solution could be simulation, which could provide a set of parameters for a sufficient number of cases to generalize the applicability of the approach.

Concerning the terrain properties, in order to correctly estimate contacts, GRFs need to be projected on the local plane where the foot is experiencing the contact. Although this can be done in first approximation by fitting a plane through the current or recent stance feet positions, more sophisticated methods (using exteroception) are required when the terrain inclination changes significantly within the support region. Other terrain properties, like elasticity or plasticity, are not explicitly accounted for, but a contact model for specific terrain classes can be learned through the proposed approach.

### VIII. CONCLUSION AND FUTURE WORK

In this paper we presented a novel probabilistic approach to contact estimation for state estimation of dynamic legged robots without contact sensing. The approach uses a logistic classifier to learn the GRF threshold which has the highest probability so as to minimize the base velocity error. Additionally, we presented an algorithm to probabilistically merge the contributions of the individual legs to create the main measurement update for our combined filter [11].

We have demonstrated that the combination of these two algorithms can double the performance in position and velocity, compared to standard methods, and compensate for a lack of dedicated contact sensors at the feet.

The presented methodology was developed and extensively tested with more than one hour of testing data from a quadrupedal robotic platform without contact sensors, in both quasi-static and dynamic locomotion regimes.

Our future work includes the integration of exteroceptive modules to further improve the performance during field trials. It would also be interesting to extend our approach to robots equipped with contact sensors so as to provide redundancy in case of sensor noise or damage.

### ACKNOWLEDGMENT

We would like to thank Roy Featherstone, Michele Focchi, and the rest of the Dynamic Legged System Lab for the valuable help with the manuscript. This work was supported by Istituto Italiano di Tecnologia (IIT).

### REFERENCES

- [1] G. P. Roston and E. Krotkov, "Dead Reckoning Navigation for Walking Robots," Robotics Institute, Pittsburgh, PA, Tech. Rep. CMU-RI-TR-91-27, Nov. 1991.
- [2] P. Sardain and G. Bessonnet, "Forces acting on a biped robot. Center of pressure-zero moment point," *Systems, Man and Cybernetics, Part A: Systems and Humans*, *IEEE Transactions on*, vol. 34, no. 5, pp. 630–637, 2004.
- [3] A. Bowling, "Impact forces and mobility in legged robot locomotion," in *IEEE/ASME International Conference on Advanced Intelligent Mechatronics*, Sept 2007, pp. 1–8.
- [4] C. Semini, N. G. Tsagarakis, E. Guglielmino, M. Focchi, F. Cannella, and D. G. Caldwell, "Design of HyQ— a hydraulically and electrically actuated quadruped robot," *Proceedings of the Institution of Mechanical Engineers, Part I: Journal of Systems and Control Engineering*, 2011.
- [5] P.-C. Lin, H. Komsuoglu, and D. E. Koditschek, "Sensor data fusion for body state estimation in a hexapod robot with dynamical gaits," *IEEE Transactions on Robotics*, vol. 22, no. 5, pp. 932–943, 2006.
- [6] M. Görner and A. Stelzer, "A leg proprioception based 6 DOF odometry for statically stable walking robots," *Autonomous Robots*, vol. 34, no. 4, pp. 311–326, 2013.
- [7] A. Chilian, H. Hirschl, and M. Görner, "Multisensor data fusion for robust pose estimation of a six-legged walking robot," in *IEEE/RSJ International Conference on Intelligent Robots and Systems (IROS)*, 2011, pp. 2497–2504.
- [8] M. Bloesch, M. Hutter, M. Hoepflinger, S. Leutenegger, C. Gehring, C. D. Remy, and R. Siegwart, "State Estimation for Legged Robots - Consistent Fusion of Leg Kinematics and IMU," in *Proceedings of Robotics: Science and Systems*, Sydney, Australia, July 2012.
- [9] M. Hutter, C. Gehring, M. Bloesch, M. A. Hoepflinger, C. D. Remy, and R. Siegwart, "StarLETH: A compliant quadrupedal robot for fast, efficient, and versatile locomotion," in *15th International Conference on Climbing and Walking Robots (CLAWAR)*, 2012.
- [10] M. Bloesch, C. Gehring, P. Fankhauser, M. Hutter, M. Hoepflinger, and R. Siegwart, "State estimation for legged robots on unstable and slippery terrain," in *IEEE/RSJ International Conference on Intelligent Robots and Systems (IROS)*, Nov 2013, pp. 6058–6064.
- [11] M. Fallon, M. Antone, N. Roy, and S. Teller, "Drift-free humanoid state estimation fusing kinematic, inertial and LIDAR sensing," in *14th IEEE-RAS International Conference on Humanoid Robots (Humanoids)*, Nov 2014, pp. 112–119.
- [12] E. Parr, "Digital Control Systems," in *Electrical Engineer's Reference Book*, 16th ed., M. Laughton and D. Warne, Eds. Newnes, 2003, pp. 1 – 36.
- [13] M. Frigerio, J. Buchli, D. G. Caldwell, and C. Semini, "RobCoGen: a code generator for efficient kinematics and dynamics of articulated robots, based on Domain Specific Languages," *Journal of Software Engineering for Robotics (JOSER)*, vol. 7, no. 1, pp. 36–54, 2016.
- [14] J. Ma, M. Bajracharya, S. Susca, L. Matthies, and M. Malchano, "Real-time pose estimation of a dynamic quadruped in GPS-denied environments for 24-hour operation," *The International Journal of Robotics Research*, 2015.
- [15] A. D. Luca, A. Albu-Schaffer, S. Haddadin, and G. Hirzinger, "Collision Detection and Safe Reaction with the DLR-III Lightweight Manipulator Arm," in *IEEE/RSJ International Conference on Intelligent Robots and Systems (IROS)*, Oct 2006, pp. 1623–1630.
- [16] S. Haddadin, A. Albu-Schaffer, A. D. Luca, and G. Hirzinger, "Collision detection and reaction: A contribution to safe physical Human-Robot Interaction," in *IEEE/RSJ International Conference on Intelligent Robots and Systems (IROS)*, Sept 2008, pp. 3356–3363.
- [17] J. Hwangbo, C. D. Bellicoso, P. Fankhauser, and M. Hutter, "Probabilistic Foot Contact Estimation by Fusing Information from Dynamics and Differential/Forward Kinematics," in *IEEE/RSJ International Conference on Intelligent Robots and Systems (IROS)*, Oct 2016.
- [18] J. Diebel, "Representing Attitude: Euler Angles, Unit Quaternions, and Rotation Vectors," 2006.
- [19] R. Featherstone, *Robot Dynamics Algorithms*. Kluwer Academic Publishers, 1987.
- [20] M. A. Hoepflinger, M. Hutter, C. Gehring, M. Bloesch, and R. Siegwart, "Unsupervised identification and prediction of foothold robustness," in *IEEE International Conference on Robotics and Automation (ICRA)*, May 2013, pp. 3293–3298.
- [21] I. Havoutis, J. Ortiz, S. Bazeille, V. Barasuol, C. Semini, and D. G. Caldwell, "Onboard perception-based trotting and crawling with the hydraulic quadruped robot (HyQ)," in *IEEE/RSJ International Conference on Intelligent Robots and Systems (IROS)*, 2013, pp. 6052–6057.
- [22] V. Barasuol, J. Buchli, C. Semini, M. Frigerio, E. R. D. Pieri, and D. G. Caldwell, "A reactive controller framework for quadrupedal locomotion on challenging terrain," in *IEEE International Conference on Robotics and Automation (ICRA)*, May 2013, pp. 2554–2561.
- [23] E. Olson, in *IEEE/RSJ International Conference on Intelligent Robots and Systems (IROS)*, Oct 2010, pp. 1059–1064.
- [24] A. Savitzky and M. J. E. Golay, "Smoothing and Differentiation of Data by Simplified Least Squares Procedures," *Analytical Chemistry*, vol. 36, no. 8, pp. 1627–1639, 1964.
- [25] C. Semini, V. Barasuol, J. Goldsmith, M. Frigerio, M. Focchi, Y. Gao, and D. G. Caldwell, "Design of the Hydraulically-Actuated, Torque-Controlled Quadruped Robot HyQ2Max," *IEEE/ASME Transactions on Mechatronics*, 2016.